POLITECNICO
MILANO 1863

RE.PUBLIC@POLIMI
Research Publications at Politecnico di Milano

Post-Print

This is the accepted version of:

C. Paravan, A. Verga, F. Maggi, L. Galfetti
Accelerated Ageing of Micron- and Nano-Sized Aluminum Powders: Metal Content, Composition and Non-Isothermal Oxidation Reactivity
Acta Astronautica, Vol. 158, 2019, p. 397-406
doi:10.1016/j.actaastro.2018.08.001

The final publication is available at https://doi.org/10.1016/j.actaastro.2018.08.001

Access to the published version may require subscription.

When citing this work, cite the original published paper.

© 2019. This manuscript version is made available under the CC-BY-NC-ND 4.0 license
http://creativecommons.org/licenses/by-nc-nd/4.0/

Permanent link to this version
http://hdl.handle.net/11311/1069390

Accelerated Ageing of Micron- and Nano-sized Aluminum Powders: Metal Content, Composition and Non-isothermal Oxidation Reactivity

Christian Paravan[a]*, Alberto Verga[b], Filippo Maggi[c], and Luciano Galfetti[d]

[a] *Department of Aerospace Science and Technology, Politecnico di Milano, 34 via LaMasa, I-20156, Milan, Italy,* christian.paravan@polimi.it
[b] *Department of Aerospace Science and Technology, Politecnico di Milano, 34 via LaMasa, I-20156, Milan, Italy,* alberto1.verga@mail.polimi.it
[c] *Department of Aerospace Science and Technology, Politecnico di Milano, 34 via LaMasa, I-20156, Milan, Italy,* filippo.maggi@polimi.it
[d] *Department of Aerospace Science and Technology, Politecnico di Milano, 34 via LaMasa, I-20156, Milan, Italy,* luciano.galfetti@polimi.it
* Corresponding Author

Abstract

Nano-sized Al (nAl) is an attractive candidate for the performance enhancement of current solid propellant formulations, and its characteristics are relevant for the development of innovative solid fuels for hybrid rocket propulsion. Nano-sized Al powders feature a higher reactivity than their micron-sized counterpart. While desirable for effective energy conversion during the combustion, this characteristic yields possible powder storage issues. This paper investigates the ageing behavior of air-passivated nAl powders under two different relative humidity conditions (RH) of 80% and 10%. Fresh and aged powders are characterized by active metal content determination (C_{Al}), electron microscopy, X-ray diffraction, and thermal analysis. The marked sensitivity of nAl (40 nm) to ageing is testified by a nearly full C_{Al} loss in just 24 hours (with RH = 80%). Under the same condition, the conventional 30 μm-counterpart loses only 13% of the original active metal content in a time of 336 hours.

Keywords: nano-sized aluminum; micron-sized aluminum; reactivity; metal content; ageing.

Nomenclature

a_s	=	mean particle diameter from specific surface area (see Eq. 1), nm
$a_{\delta,Al2O3}$	=	calculated oxide layer thickness (see Eq. 2), nm
C_{Al}	=	active Al content (by mass), %
D_{32}	=	surface-based mean diameter, nm
D_{43}	=	mass-based mean diameter, nm
nAl	=	nano-sized Al powder
nAl-40	=	nAl with nominal size of 40 nm
nAl-100	=	nAl with nominal size of 100 nm
RH	=	relative humidity, %
SSA	=	specific surface area, m^2/g
t	=	time
T	=	temperature, K
$T_{end,i}$	=	i-th intense oxidation end temperature, K
$T_{onset,i}$	=	i-th intense oxidation onset temperature, K
$\alpha_{Al\rightarrow Al2O3}(T)$	=	$Al\rightarrow Al_2O_3$ conversion factor at temperature T, $\Delta m(T)/(C_{Al}\cdot 0.89)$, %
$\alpha_{Al\rightarrow Al(OH)3}(t)$	=	$Al\rightarrow Al(OH)_3$ conversion factor at time t, $\Delta m(t)/(C_{Al}\cdot 1.889)$, %
Δm_0	=	mass change due to adsorbed species desorption, %
Δm_1	=	mass change in the first oxidation step, %
Δm_{933K}	=	mass change at 933 K, %
Δm_{1223K}	=	mass change at 1223 K, %
μAl	=	micron-sized Al powder
μAl-7.5	=	μAl with nominal size of 7.5 μm
μAl-30	=	μAl with nominal size of 30 μm
ρ	=	density, kg/m^3

1. Introduction

Aluminum powders are widely used in condensed energetic systems [1–3] and, in particular, in mature solid propellant formulations and innovative solid fuels for rocket applications [4–6]. Typically, Al particles are passivated by air and present a layered structure with a metal core surrounded by an amorphous Al_2O_3 shell. The Al_2O_3 layer prevents the fast Al reaction with the surrounding environment at ambient conditions. Currently, commercial solid propellants are based on air-passivated μAl. The key features of micron-sized Al powders are active aluminum content (C_{Al}) typically higher than 95 wt%, and specific surface area (SSA) lower than 1 m^2/g. The μAl grants a high theoretical energy content, but its relatively low SSA yields limited reactivity (i.e., high ignition temperature [7]). Nano-sized Al powders feature increased reactivity over the conventional μAl [8–10]. In particular, air-passivated nAl shows higher SSA (≥ 10 m^2/g), and a lower C_{Al} (< 90 wt%) than μAl. While attractive in terms of the enhanced performance in a combustion environment, nAl high reactivity may yield issues related to powder ageing under storage (i.e., C_{Al} reduction, alteration of the initial composition). Table 1 shows the effects of powder C_{Al} decrease on the flame temperature (T_{fl}) and theoretical vacuum specific impulse ($I_{s,vac}$) of a typical commercial aluminized solid propellant based on ammonium perchlorate (AP, 68 wt%),with hydroxyl-terminated polybutadiene (HTPB, 14 wt%) and a metal powder content of 18 wt%. The calculations are performed by NASA CEA code [11], with data that are evaluated considering different C_{Al} for the metal powder. The C_{Al} is varied in the range 100% (ideal case, assuming the absence of the Al_2O_3 layer) to 50%. The C_{Al} reduction is achieved assuming that in the powder the remainder of the metal is its oxide (Al_2O_3). The theoretical $I_{s,vac}$ for the metallized propellant formulations shows a nearly linear dependence from the powder C_{Al}.

Table 1. Theoretical performance of non-metallized/aluminized solid propellant formulations (NASA CEA Code, chamber pressure 7.0 MPa, expansion ratio 40, shifting equilibrium, HTPB heat of formation from [12]).

Al Powder Mass Fraction, wt%	**C_{Al}, wt%**	**T_{fl}, K**	**$I_{s,vac}$, s**	**$\Delta I_{s,vac}$, %**
0 [a]	-	1372	239.1	-
0 [b]	-	2890	287.4	-
18	100	3382	314.4	0.0
	95	3349	311.5	-0.9
	90	3312	308.6	-1.8
	80	3229	302.6	-3.8
	70	3133	296.2	-5.8
	60	3026	289.5	-7.9
	50	2909	282.6	-10.1

[a] Non-metallized formulation with O/F = 2.125: AP (68 wt%), HTPB (32 wt%). [b] Non-metallized formulation with O/F = 6.143: binder content is the same as per the metallized formulations (HTPB, 14 wt%), while the AP mass fraction is increased (86 wt%).

The same working hypotheses are used for the evaluation of the T_{fl} and $I_{s,vac}$ in O_2 of HTPB + 10 wt% Al solid fuel formulation, for $1.5 \leq O/F \leq 3.5$ (see Figure 1). In this case, a O/F range is considered to provide an insight of the performance changes due to the oxidizer-to-fuel ratio shift [13]. In commercial solid propellants, high density energetic additives as μAl are added mainly to improve the specific impulse of the system (see Table 1), with a crucial role played by C_{Al}. In solid fuel formulations metal particles are exploited to augment the heat transfer from the flame zone to the condensed phase, with the final aim of increasing the regression rate. Thus, in solid fuel formulations energetic

filler reactivity plays a key role, with limited impact of the active metal content [2,3]. Data reported in Figure 1 testify this effect. The additive C_{Al} reduction yields faint T_{fl} and $I_{s,vac}$ detriment (under the same working hypotheses of the Table 1 data). The impact of the powder C_{Al} on $I_{s,vac}$ is stronger for solid propellants than for solid fuel formulations. On the other hand, the metal powder reactivity (not captured by the chemical equilibrium analysis) plays a key role in the determination of burning rates of condensed materials, and on the formation of aggregates/agglomerates [2–4,14–16]. Thus, not only the active metal content of the Al powder should be considered for an evaluation of its effects on the condensed energetic material, but also the additive reactivity (i.e., residual C_{Al}, its intense oxidation onset temperature and its ability to be exothermically converted to the metal oxide). Both initial particle size (μAl vs. nAl) and ageing characteristics (i.e., surface composition and permeability) play a significant role in the understanding of the energetic filler effects on the ballistic response of different systems [17,18].

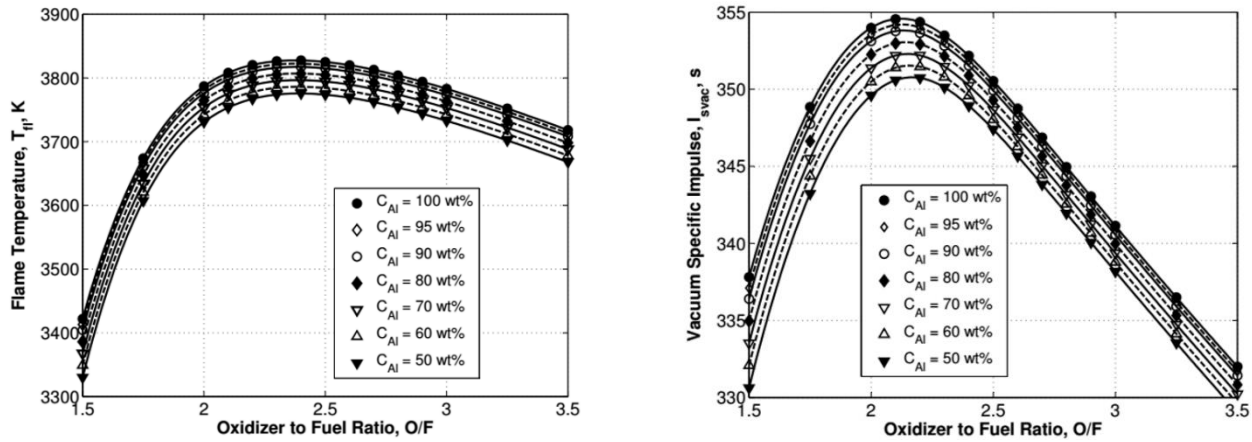

a **b**

Figure 1. Theoretical performance of HTPB + 10 wt% Al fuel formulation burning in O_2 effects of the powder C_{Al} on (a) T_{fl}(O/F) and (b) $I_{s,vac}$(O/F) (NASA CEA Code, chamber pressure 7.0 MPa, expansion ratio 40 shifting equilibrium, HTPB heat of formation from [12], initial oxidizer temperature 90 K).

This paper investigates the accelerated ageing behavior of aluminum powders with various particle sizes. The samples are stored under different relative humidity conditions. Tested powders range from conventional μAl to nAl. All the tested powders are passivated by air. Implemented diagnostics include: scanning and transmission electron microscopy (SEM/TEM), X-ray diffraction (XRD), C_{Al} determination, sample weight monitoring in time and low heating rate reactivity analysis by thermogravimetry (TG). The collected information shows the ageing effects on powder energetic content (C_{Al}) and reactivity.

1.1 Literature Survey

In the open-literature, few studies deal with the ageing process of Al powders [19–22]. On the other hand, Al ageing effects (under non fully controlled/reported conditions) are observed in different publications [17,23–25]. Cliff et al. tested air passivated nAl (C_{Al} = 88.2%, SSA = 12.7 m^2/g). Under RH = 75%, and temperatures of 333 K, the air-passivated nAl powder showed a C_{Al} drop to 4% in a time span of 40 days [19]. Li et al. performed accelerated ageing tests under T = 303 K, for different RH levels (10-20%, 50-60%, and 80-90%) for a period of 8 weeks [20]. In the study, no details on the starting air-passivated nAl powders were given. High-resolution TEM images showed the growth of the passivation layer shell around the particles from 3 to 5 nm, because of the ageing process. DSC-TG analyses testified a non-clear trend of the oxidation behavior of the tested materials, though the two-step oxidation behavior of nAl was recognized over both fresh and aged specimens. A long-term study on nAl ageing (RH = 60-80%, T = 293-298 K) was performed by Nazarenko et al. [21]. In this study, nAl powders were stored for a period of at least 10 years. Non-isothermal oxidation tests revealed that aged powders reactivity was quite similar to the one of fresh counterpart, with an overall heat release of 8.5 kJ/g, for a C_{Al} = 71%. Pisharath et al. tested the accelerated ageing behavior of air-passivated and functional organic silane-passivated nAl powders. Detailed X-ray photoelectron spectroscopy (XPS) and TG analyses evidenced the effective deposition of the chemical passivation layer, that promoted an improved ageing resistance than the pristine Al_2O_3-shell [22]. Cerri et al. contrasted the nAl metal content loss in solid propellant formulations with the behavior of μAl-loaded compositions, showing a marked effect of powder

size reduction on the Al corruption [26]. Achieved results show a faster degradation of the C_{Al} of formulations doped with nano-sized metal powders.

2. Materials and Experimental Methods

2.1 Tested Powders

Micron- and nano-sized air-passivated powders were considered in the study. Micron-sized powders have spherical shape and nominal sizes of 30 and 7.5 μm (μAl-30, and μAl-7.5 respectively), and are produced by AMG Alpoco (UK). The nAl powders are obtained by electrical explosion of wires [27]. The nAl-100 (nominal size 100 nm) is produced by Advanced Powder Technology (APT) LLC (Russia), while nAl-40 is supplied by US Nanomaterials (USA).

2.2 Powder Characterization

Powder particle size distribution was determined by laser granulometry (Malvern Mastersizer 2000). The SSA was determined from N_2 adsorption/desorption isotherms [28]. The average particle size was evaluated by two different approaches: laser granulometry (D_{43} and D_{32} from Malvern Mastersizer 2000) and calculations based on the SSA of the powders. In particular, the SSA-based particle size (a_s) and the corresponding alumina layer thickness based on the measured C_{Al} ($a_{\delta,Al2O3}$) are calculated by the Eqs. 1-2 [8] (ρ_{Al} = 2700 kg/m^3, and $\rho_{Al2O3(amorphous)}$ = 3050 kg/m^3)

$$a_s = 6/(\rho_{Al}\, SSA) \tag{1}$$

$$a_{\delta,Al2O3} = \frac{a_s}{2} - \left[\frac{\rho_{Al2O3(amorphous)} \cdot C_{Al} \cdot (a_s/2)^3}{\rho_{Al} \cdot (1 - C_{Al}) + \rho_{Al2O3(amorphous)} \cdot C_{Al}}\right]^{1/3} \tag{2}$$

Particle morphology and structure were evaluated by SEM and TEM. The C_{Al} was determined by H_2 volume evolution from Al + H_2O reaction [3,10]. Crystalline phases were identified by XRD. Thermogravimetric analyses were performed in air, with heating rate of 10 K/min. Powder reactivity was determined exploiting the parameters suggested by Ilyin et al. [8], and a modified intense oxidation onset temperature, $T_{onset,1+}$. The latter is defined as the temperature corresponding to a mass increase of 1% for the tested sample, after the maximum mass loss (Δm_0), see Figure 2.

2.3 Accelerated Ageing

Accelerated ageing was studied on small samples of powders (< 1 g). Specimens were prepared in glass weighting bottles with diameter of 30 mm. The relatively low amount of material granted a uniform exposure to the test environment. The open weighting bottles were placed in small plastic jars and were then inserted in pre-prepared sealed glass vessels containing the test environments. Different RH conditions were produced by H_2O saturated salt solutions/silica granules (see Table 2). The plastic jar prevented the contact between the weighting bottles and the salt solution/silica. The sealed glass vessels were prepared and stored at the test temperature 24-48 hours before the start of the experiments. The investigated RH were < 10% (dry air condition) and (80.2 ± 0.4)%. A single temperature of 333 K is considered in the study. In the humid ageing analyses, the Al→$Al(OH)_3$ conversion factor was defined as a function of the ageing time, similarly to the $\alpha_{Al\rightarrow Al2O3}$(T) defined in TG analyses [8], as shown in the Eq. 3

$$\alpha_{Al\rightarrow Al(OH)3}(t) = \Delta m(t)/(C_{Al} \cdot 1.889) \tag{3}$$

Table 2. Investigated ageing conditions, dry and wet environments RH and temperature.

Condition Id.	Temperature, K	RH, %	Notes
Dry, D1	333	< 10	Dry air environment by SiO_2
Humid, H1	333	80.2 ± 0.4	Saturated H_2O + KCl solution

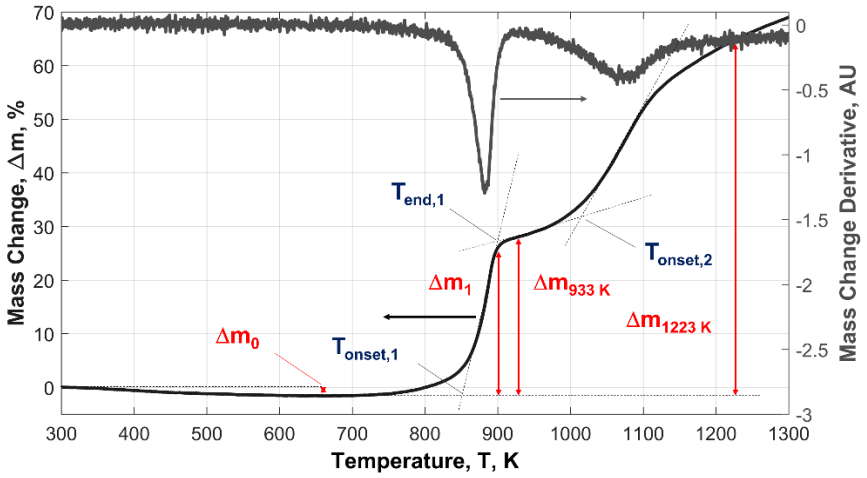

a

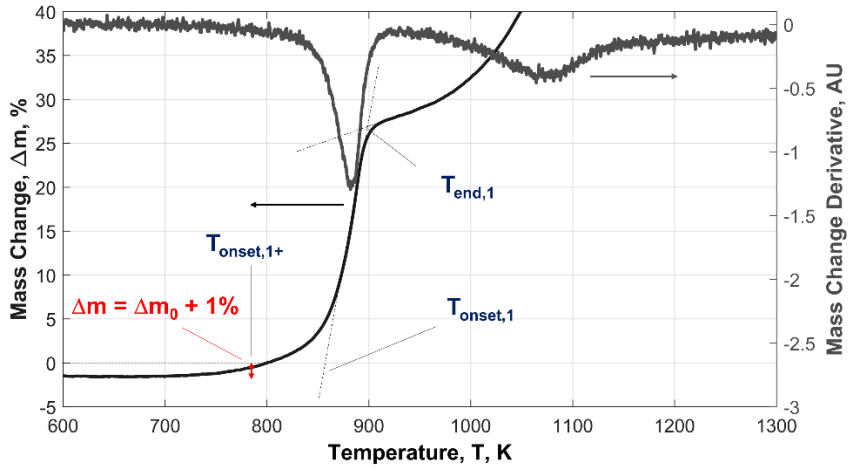

b

Figure 2. Identification of reactivity parameters from TG and differential TG (DTG) curves: (a) parameters typically considered in the open literature are due to Ilyin et al. [8], (b) detail for the $T_{onset,1+}$ definition.

3. Experimental Results

3.1 Initial Characterization

The tested powders and their relevant size data are presented in the Table 3. Micron-sized powders feature low SSA values, yielding high a_s, as confirmed by the D_{43} and D_{32} (see Table 3). The relatively low C_{Al} of the μAl-7.5 is partially due to the reduced size with respect to μAl-30, testified by the lower average mass-based diameter (D_{43}). While μAl-30 exhibits a monomodal size distribution, μAl-7.5 is slightly bimodal and features a small volume fraction of particles (~ 2 vol.%) in the sub-micrometric range (0.4-1 μm). Nano-sized particles show high SSA and reduced a_s. Considering the nAl C_{Al}, the Al_2O_3 shell thickness is in the range 3-4 nm [29]. The a_s of the nAl-100 is nearly doubled with respect to the nAl-40. XRD analyses performed on the powders revealed metallic Al as the unique crystalline phase in the materials (see Figure 3). This means that the presence of other crystalline phases (as Al_2O_3 polymorphs), if any, is limited by the hardware measurement threshold (< 5%).

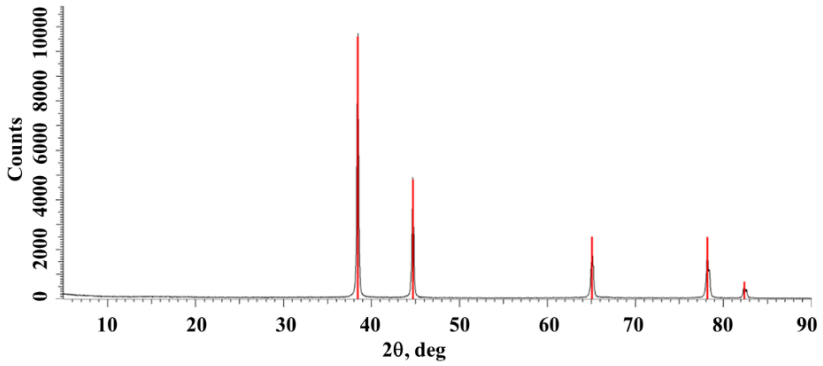

Figure 3. Typical XRD result for the investigated powders (nAl-40). The only recognized crystalline phase is Al.

Scanning electron microscope image of the μAl-30 is shown in Figure 4. This powder features mainly spheroid particles, with some non-spherical granules. In general, the particle texture appears relatively smooth, and clustering is nearly absent (due to the reduced SSA). The SEM and the TEM of the nano-sized powders are reported in the Figure 5 and Figure 6, respectively. These electron microscope images show a relatively uniform circular shape of the particles (with few exceptions in the nAl-40, see Figure 6). This grants a relatively high confidence on the a_s and $a_{\delta,Al2O3}$ data presented in the Table 3. The Al_2O_3 layer surrounding the nAl particles appears amorphous in the TEM images (i.e., absence of a well ordered structure), thus confirming the XRD results (see Figure 3).

The TG traces for the non-isothermal oxidation of the powders are reported in the Figure 7, while reactivity parameters are presented in the Table 4. Micron-sized particles exhibit limited reactivity under the investigated conditions. In particular, considering the low temperature oxidation of the powders, the $T_{onset,1}$ of μAl-30 is (865.0 ± 0.3) K, with $\Delta m_{933\ K}$ = (0.5 ± 0.3)%. While for the finer μAl, the first intense oxidation onset temperature is (842.5 ± 0.5) K, and $\Delta m_{933\ K}$ = (1.8 ± 0.5)%. For the two powders, $T_{onset,1+}$ captures the limited oxidation reactivity (see Table 4). The limiting Al→Al_2O_3 conversion factor for the powders is (2.9 ± 0.2)%, for μAl-30, and (13.7 ± 0.5)% for μAl-7.5. The nAl powders show a two-step reaction process, with a first intense oxidation onset before the Al melting temperature (933 K) [8]. The $T_{onset,1}$ shows no clear correlation with the powder size, as evidenced by the intense oxidation onset temperature for the nAl-100 with respect to the μAl-7.5. This is due to the relatively slow low-temperature oxidation rate of the finer micron-sized powder, see Figure 7. The higher reactivity of the nano-sized powders is well captured by the $T_{onset,1+}$. The increased SSA of nAl-100 and nAl-40 yields an increased reactivity over the μAl-counterparts, as testified by the $\alpha_{Al\rightarrow Al2O3}$(933 K) and $\alpha_{Al\rightarrow Al2O3}$(1223 K) values. The incomplete Al conversion in Al_2O_3 during the TG runs is testified by both the monotonic increasing trend of Δm(T), and the $\alpha_{Al\rightarrow Al2O3}$ limiting values. Due to this, no definite ending point is reported for the second intense oxidation step.

Table 3. Initial characteristics of the tested μAl and nAl powders. The D_{43} and D_{32} are evaluated on a volume-based measurement. Particle size and C_{Al} results are presented as the average ensemble of three runs. The confidence interval of C_{Al} is expressed by standard deviation.

Powder Id.	**Nominal Size, nm**	**SSA, m^2/g**	**a_s, Eq. 1 nm**	**D_{43}, nm**	**D_{32}, nm**	**C_{Al}, wt.%**	**$a_{\delta,Al2O3}$, Eq. 2, nm**
μAl-30	30000	< 0.1	>22000	44200 [a]	28900 [a]	99.1 ± 0.2	NAv.
μAl-7.5	7500	< 0.1	>22000	6600 [a]	4150 [a]	95.3 ± 0.2	NAv.
nAl-100	100	12.6 ± 0.1	176	138 [b]	133 [b]	85.7 ± 0.6	3.9
nAl-40	40	24.5 ± 0.1	90.7	NAv.	NAv.	77.1 ± 0.5	3.4

[a] Measured by Malvern Mastersizer 2000 (dry dispersion unit), [b] Measured by Malvern Mastersizer 2000 (liquid dispersion unit).

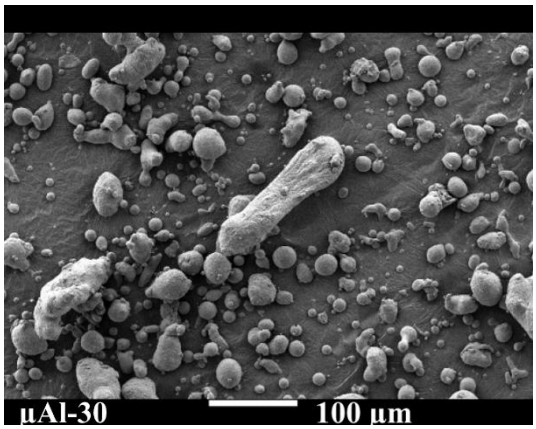

Figure 4. SEM of the μAl-30, note the presence of large, non-spherical granules and the absence of particle clustering.

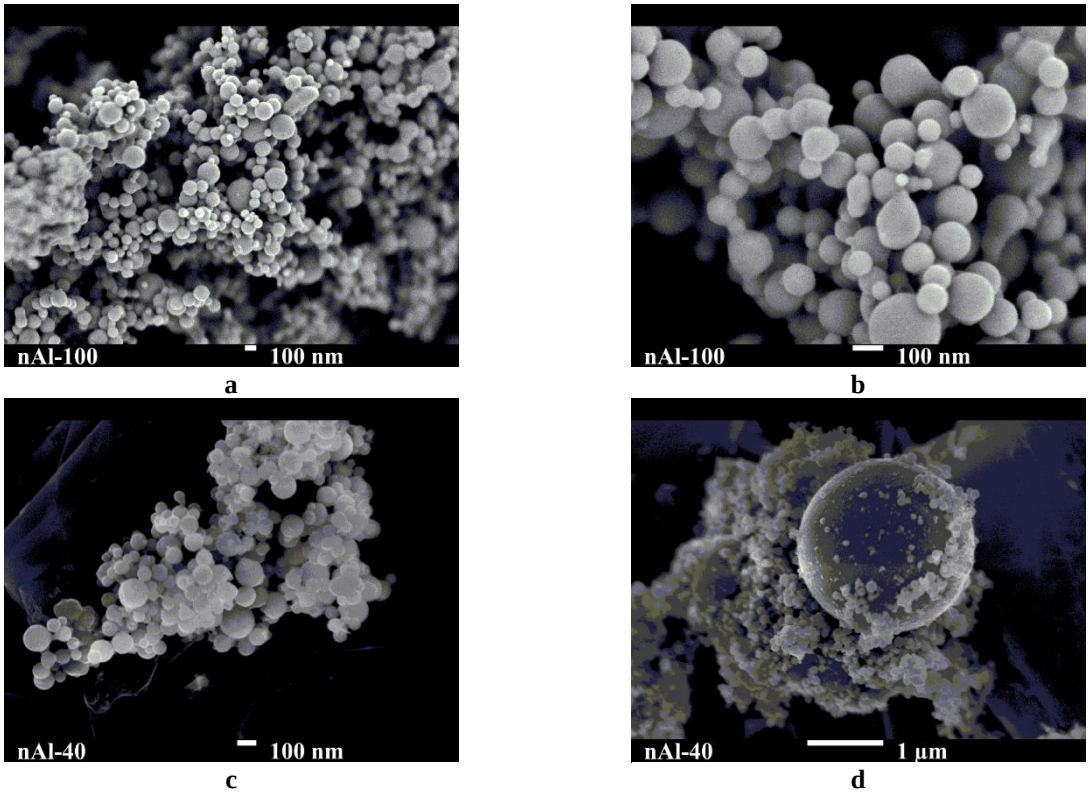

Figure 5. SEM of (a, b) nAl-100 and (c, d) nAl-40. The marked clustering tendency of nanoparticles is evident. Particle size distribution of nAl-100 appear relatively uniform, with few (if any) particles with size in the sub-micrometric range, while larger granules are observed in nAl-40, see (d).

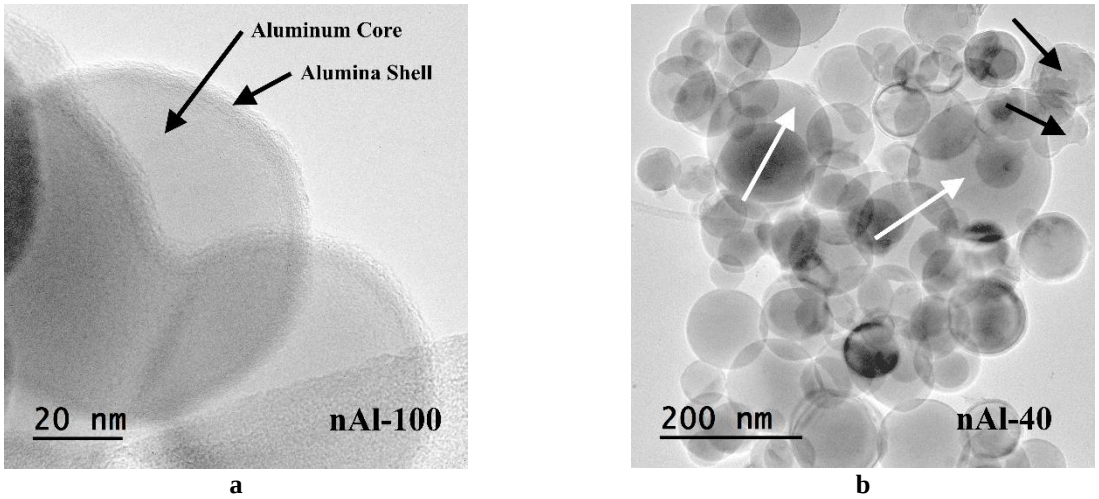

Figure 6. TEM of (a) nAl-100 and (b) nAl-40. Note the core-shell structure typical of air-passivated Al powders, and the relatively uniformity of the Al_2O_3 shell thickness. Few non-spherical elements are recognized in the nAl-40 powder (black arrows), as well as relatively large particles (white arrows).

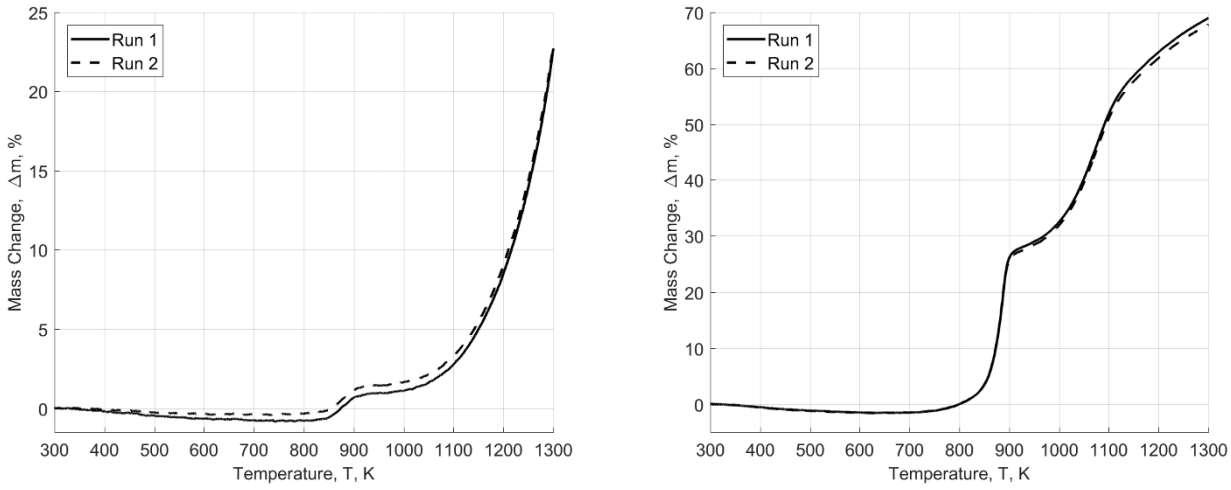

Figure 7. TG traces (air, 10 K/min, 0.1 MPa) of (a) µAl-7.5 and (b) nAl-100.

Table 4. Fresh Al powder reactivity parameters (TG, air, 10 K/min, 0.1 MPa). Interval of confidence for the two performed runs defined by standard deviation.

	µAl-30	**µAl-7.5**	**nAl-100**	**nAl-40**
Δm_0, %	-0.2 ± 0.1	-0.6 ± 0.3	-1.6 ± 0.4	-2.2 ± 0.2
$T(\Delta m_0)$, K	782.7 ± 2.1	741.2 ± 0.7	663.4 ± 1.9	608.5 ± 0.3
$T_{onset,1}$, K	865.0 ± 0.3	842.5 ± 0.5	856.1 ± 0.2	816.5 ± 1.0
$T_{onset,1+}$, K	1121.0 ± 7.1	878.4 ± 2.5	781.0 ± 0.1	742.7 ± 1.1
Δm_1, %	0.5 ± 0.1	1.8 ± 0.5	28.2 ± 0.4	28.8 ± 0.3
$T_{end,1}$, K	915.3 ± 0.6	905.2 ± 0.4	898.4 ± 0.5	866.7 ± 0.5
Δm_{933K}, %	0.5 ± 0.2	1.8 ± 0.5	29.5 ± 0.4	31.6 ± 0.2
$\alpha_{Al\rightarrow Al2O3}$(T = 933 K)	0.6 ± 0.1	2.2 ± 0.6	38.7 ± 0.6	46.1 ± 0.4
$T_{onset,2}$, K	1224.2 ± 0.4	1203.3 ± 0.4	1014.9 ± 0.5	992.8 ± 2.7
Δm_{1223K}, %	2.5 ± 0.2	11.6 ± 0.5	65.6 ± 0.8	62.4 ± 0.4
$\alpha_{Al\rightarrow Al2O3}$(T = 1223 K)	2.9 ± 0.2	13.7 ± 0.5	86.0 ± 1.1	90.9 ± 0.8

3.2 Accelerated Ageing Effects

3.2.1 Dry Environment

Tests performed under RH < 10% yield similar results for μAl and nAl powders. In particular, independently from powder SSA, no significant change in mass is observed over a period of 14 days. The relatively low H_2O content in the ageing environment limits the formation of $Al(OH)_3$ from the pristine Al_2O_3 shell. Under the investigated conditions, the alumina layer shows an effective passivation action on the metal core. Over the 14 days ageing period, the C_{Al} of μAl-30 shows no decrease. The active metal content of μAl-7.5 changes from (95.3 ± 0.2)% to (94.2 ± 0.6)%. Similarly, both the nAl-100 and the nAl-40 show no metal content changes. In particular, nAl-40 features an initial C_{Al} = (77.1 ± 0.5)% that turns to (76.5 ± 0.5)% at the end of the storage time. The 14 days ageing produces no influences on the nAl reactivity parameters, as testified by a comparison between Table 4 and Table 5 data. In particular, no intense oxidation onset temperature or $\alpha_{Al\rightarrow Al2O3}(T)$ shifts are noted for the powders. This reflects a similar behavior of the fresh and aged materials during their oxidation.

Table 5. Relevant reactivity parameters for 14 days-ageing test in dry environment (D1 condition). Interval of confidence for the two performed runs defined by standard deviation. Micron-sized powders were not tested since C_{Al} and mass of the specimen were not changed during storage (refer to Table 4 for relevant data).

	nAl-100	**nAl-40**
C_{Al}, %	85.6 ± 0.3	76.5 ± 0.5
Δm_0, %	-0.9 ± 0.1	-2.9 ± 0.3
$T(\Delta m_0)$, K	655.5 ± 0.7	640.9 ± 0.3
$T_{onset,1}$, K	857.5 ± 0.1	817.6 ± 0.5
$T_{onset,1+}$, K	775.0 ± 2.0	747.8 ± 1.9
Δm_1, %	28.4 ± 0.1	28.8 ± 0.3
$T_{end,1}$, K	898.6 ± 0.1	866.7 ± 0.1
Δm_{933K}, %	29.5 ± 0.1	31.4 ± 0.3
$\alpha_{Al\rightarrow Al2O3}$(T = 933 K), %	38.7 ± 0.2	46.2 ± 0.6
$T_{onset,2}$, K	1014.5 ± 0.5	991.0 ± 0.3
Δm_{1223K}, %	64.7 ± 0.4	60.1 ± 0.8
$\alpha_{Al\rightarrow Al2O3}$(T = 1223 K), %	84.8 ± 0.6	88.3 ± 1.3

3.2.2 Humid Environment

The humid condition created by the use of a KCl-saturated H_2O solution was investigated at 333 K (see Table 2). The specimen mass change during the ageing in the H1 condition, the $C_{Al}(t)$ and the $\alpha_{Al\rightarrow Al(OH)3}(t)$ are shown in Figure 8 for the μAl-30 and the nAl-40. The behavior of these two powders represents the typical trend of the two families of particles considered in the study. Ageing of the powders in humid condition is significantly affected by their SSA. The μAl-30 exhibits an initial decrease of the $C_{Al}(t)$, and a corresponding mass increase due to initial H_2O vapor adsorption and reaction with the powder. After 7 days (168 hrs.), the $C_{Al}(t)$ decreasing behavior disappears, and both the active metal content and the sample mass values show no further changes till the end of the tests. The active metal content of μAl-30 decreases from (99.1 ± 0.2)% to (86.8 ± 0.9)%, with a maximum mass increase of (8.9 ± 0.4)% at 14 days. The final $\alpha_{Al\rightarrow Al(OH)3}$ for this powder is (4.7 ± 0.2)%. The low $Al\rightarrow Al(OH)_3$ conversion factor testifies the relatively low reactivity of the powder in an oxidizing environment. The μAl-7.5 shows a similar behavior, with C_{Al}(168 hrs.) = (58.1 ± 0.8)%. At the end of the ageing time, this powder shows C_{Al} = (55.8 ± 0.6)%, with $\alpha_{Al\rightarrow Al(OH)3}$ = (21.3 ± 1.4)%. Contrasting the two micron-sized powders, the increased ageing sensitivity of the μAl-7.5 is due to its reduced size, and to the presence of a sub-micrometric particles fraction (see Table 3). High SSA powders (nAl-100 and nAl-40) are more prone to ageing than their micron-sized counterparts (see Figure 8). Both the nano-sized Al powders show a nearly complete C_{Al} corruption under the investigated conditions. For nAl-100, a C_{Al} drop below 50% of the initial value requires less than 30 hrs. Under the investigated conditions, the C_{Al} of nAl-100 is nearly unchanged in the first 24 hrs., and then reaches a value of (6.2 ± 0.2)% for t = 27 hrs. After 48 hrs., the active metal content of the powder is (2.3 ± 0.3)%, and the mass change has reached its limiting value (under the investigated conditions) with $\alpha_{Al\rightarrow Al(OH)3}$ = (96.3 ± 0.9)%. The ageing for the nAl-40 is faster than for the nAl-100. The whole C_{Al} corruption process requires less than 24 hrs. (see Figure 8c). The final $\alpha_{Al\rightarrow Al(OH)3}$ of the nAl-40 results (97.3 ± 1.3)%.

The mass gain during the powder ageing in a wet environment is initially due to the adsorption of H_2O on the particle surfaces. This process is then followed by the formation of hydrated species [i.e., $Al(OH)_3$] on the surface of the particles. At this point, the protective action of alumina is weakened. As a consequence, the particle core can be oxidized by the diffusion of water vapor (and other oxidizing species). The active metal content is thus consumed. The presence of crystalline aluminum oxides and hydroxides was investigated by XRD. Achieved results are reported in Table 6 and in Table 7 for micron- and nano-sized powders, respectively.

Table 6. XRD results for μAl-30 and μAl-7.5 during ageing (H1 condition).

	Time, days	**Al, %**	**$Al(OH)_3$, %**		
			Bayerite	**Boehmite**	**Nordstrandite**
μAl-30	0	100	-	-	-
	7	96.9	2.8	-	0.3
μAl-7.5	0	100	-	-	-
	7	71.9	22.3	-	5.8

Table 7. XRD results for nAl-100 and nAl-40 during ageing (H1 condition).

	Time, hours	Al, %	$Al(OH)_3$, %		
			Bayerite	Boehmite	Nordstrandite
nAl-100	0	100	-	-	-
	36	4.3	59.2	24.2	12.3
	72	2.7	68.2	22.0	7.1
nAl-40	0	100	-	-	-
	24	3.0	51.9	38.2	6.9

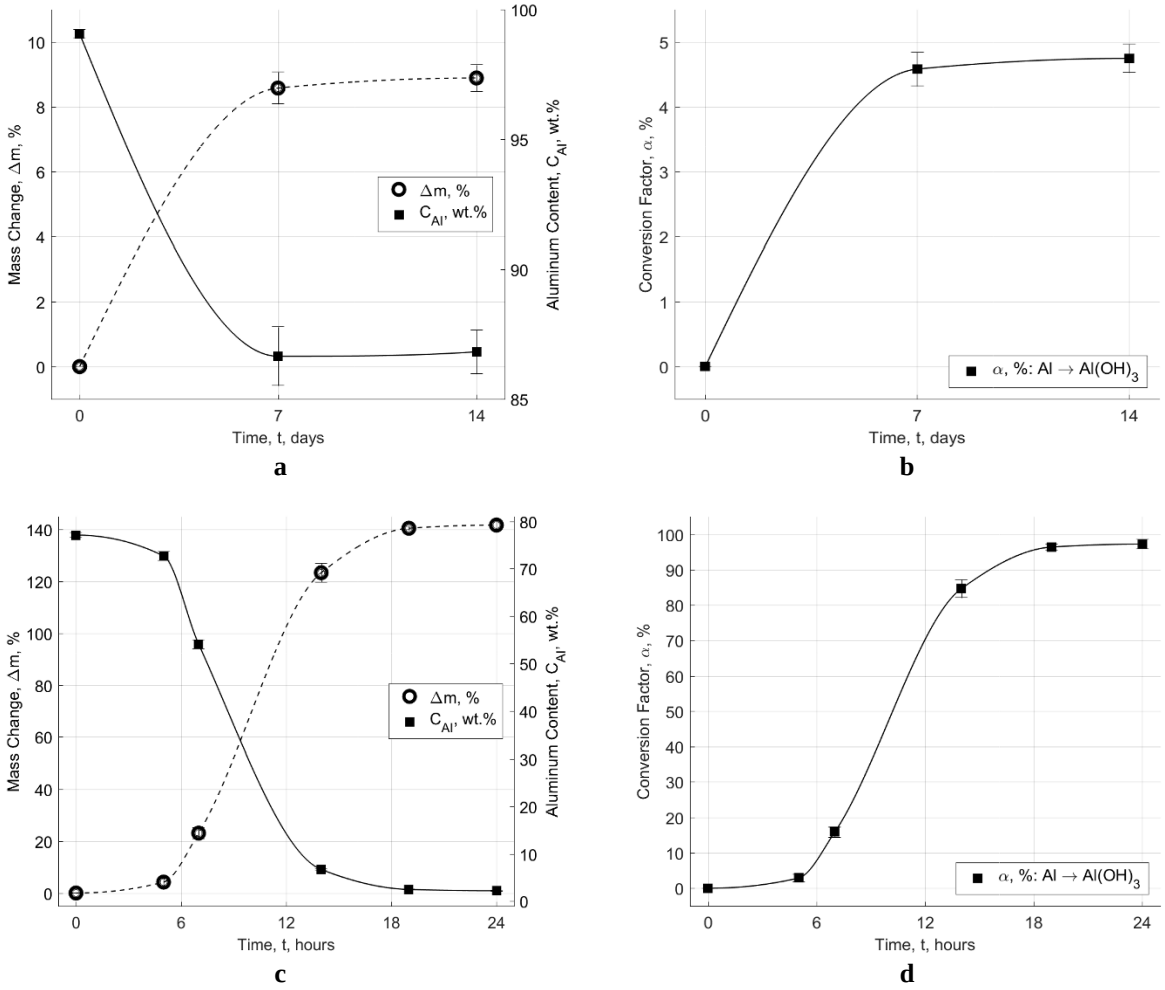

Figure 8. Evolution in time during accelerated ageing (H1 condition) of $\Delta m(t)$, $C_{Al}(t)$ and $\alpha_{Al \rightarrow Al(OH)3}(t)$ for (a, b) µAl-30 and (c, d) nAl-40. Interval of confidence is defined by standard deviation, data interpolating lines are reported for improved readability.

The crystallographic data evidence the different $Al(OH)_3$ polymorphs (bayerite, boehmite, and nordstrandite) in the aged specimens. The XRD traces show a good qualitative agreement with the achieved ageing mass changes (see Figure 8). Under the investigated conditions, no boehmite was identified in the micron-sized Al corruption products, with this aluminum hydroxide polymorph that was identified only for the nAl-100 and nAl-40. The composition changes yield modifications in the morphology of the particles of the powders. In particular, the SEM images reported in Figure 9 testify the marked clustering tendency of the aged powders. Due to the powder alterations, yielding large sizes and thicknesses of the particles/clusters, no TEM images could be captured for the aged nAl specimens. The micron-sized powders feature a non-smooth texture, while nAl shows the presence of non-spherical elements.

Table 8. Reactivity parameters for TG analyses (air, 10 K/min, 0.1 MPa) of µAl-30 and µAl-7.5 during ageing (H1 condition). Interval of confidence is defined by standard deviation over the two performed runs.

	µAl-30		**µAl-7.5**	
	168 hrs.	**336 hrs.**	**168 hrs.**	**336 hrs.**
Δm_0, %	-3.7 ± 0.1	-4.3 ± 0.1	-13.1 ± 0.1	-13.9 ± 0.2
$T(\Delta m_0)$, K	790.8 ± 0.4	800.7 ± 0.5	815.8 ± 1.1	816.2 ± 0.5
$T_{onset,1}$, K	905.1 ± 1.4	895.9 ± 0.6	884.4 ± 1.9	884.3 ± 0.3
$T_{onset,1+}$, K	NAv.	NAv.	925.5 ± 0.9	978.0 ± 2.5
Δm_1, %	0.4 ± 0.2	0.4 ± 0.3	1.0 ± 0.1	0.9 ± 0.3
$T_{end,1}$, K	937.0 ± 0.1	936.2 ± 1.3	928.1 ± 1.4	928.0 ± 0.5
Δm_{933K}, %	0.3 ± 0.2	0.4 ± 0.2	1.1 ± 0.1	1.0 ± 0.3
$\alpha_{Al\rightarrow Al2O3}(T = 933\ K)^a$	0.4 ± 0.2	0.6 ± 0.3	2.1 ± 0.1	1.9 ± 0.6
$T_{onset,2}$, K	1215.5 ± 1.8	1206.2 ± 0.1	1191.7 ± 0.8	1189.6 ± 1.2
Δm_{1223K}, %	1.4 ± 0.2	1.9 ± 0.4	4.7 ± 0.2	4.3 ± 0.3
$\alpha_{Al\rightarrow Al2O3}(T = 1223\ K)^a$	1.8 ± 0.3	2.4 ± 0.6	9.1 ± 0.3	8.6 ± 0.6

[a] Based on the C_{Al} from the volumetric analysis of the Al + H_2O reaction.

Table 9. Reactivity parameters for TG analyses (air, 10 K/min, 0.1 MPa) of nAl-100 and nAl-40 during ageing (H1 condition). Interval of confidence is defined by standard deviation over the two performed runs.

	nAl-100			**nAl-40**	
	24 hrs.	**27 hrs.**	**72 hrs.**	**7 hrs.**	**24 hrs.**
Δm_0, %	-2.1 ± 0.2	-30.2 ± 0.5	-32.1 ± 0.2	-9.6 ± 0.2	-31.9 ± 0.1
$T(\Delta m_0)$, K	655.3 ± 0.1	837.6 ± 2.1	1053.1 ± 1.4	654.3 ± 0.7	1021.4 ± 2.3
$T_{onset,1}$, K	857.6 ± 0.5	860.7 ± 0.4	NAv.	814.3 ± 0.1	NAv.
$T_{onset,1+}$, K	776.7 ± 3.6	NAv.	NAv.	749.4 ± 1.2	NAv.
Δm_1, %	27.4 ± 0.7	0.6 ± 0.7	NAv.	21.2 ± 0.3	NAv.
$T_{end,1}$, K	899.3 ± 0.3	899.3 ± 0.6	NAv.	866.6 ± 1.0	NAv.
Δm_{933K}, %	28.5 ± 0.6	0.6 ± 0.8	0.2 ± 0.2	22.7 ± 0.3	0.2 ± 0.0(3)
$\alpha_{Al\rightarrow Al2O3}$(T = 933 K)[a]	37.5 ± 0.9	10.9	10.0	47.1 ± 1.0	9.7 ± 1.9
$T_{onset,2}$, K	1015.5 ± 0.4	1016.7 ± 0.8	NAv.	989.7 ± 0.7	NAv.
Δm_{1223K}, %	62.6 ± 1.1	2.1 ± 0.8	0.1 ± 0.2	41.9 ± 0.3	0.1 ± 0.0(5)
$\alpha_{Al\rightarrow Al2O3}$(T = 1223 K)[a]	82.5 ± 1.5	38.2	10.6	87.0 ± 1.6	9.7 ± 2.4

[a] Based on the C_{Al} from the volumetric analysis of the Al + H_2O reaction.

Table 8 and Table 9 report the reactivity parameters for low temperature oxidation of aged micron- and nano-sized powders. Both micron-sized powders exhibit limited changes on their low-heating rate reactivity after ageing (see Table 4 and Table 8). With respect to the fresh powder, the aged μAl-30 shows nearly unchanged $\alpha_{Al\rightarrow Al2O3}$, due to the reductions of C_{Al} and $\Delta m(T)$. On the other hand, intense oxidation temperatures rise for the aged powders from $T_{onset,1}$ = (865.0 ± 0.3) K to (895.9 ± 0.6) K. Ageing effects are more intense for μAl-7.5. This powder features $T_{onset,1}$ and $T_{onset,1+}$ increases (see Table 4 and Table 8). After 336 hrs. of ageing, μAl-7.5 shows $\alpha_{Al\rightarrow Al2O3}$(1223 K) reduction from (13.7 ± 0.5)% to (8.6 ± 0.6)%. This reactivity reduction of the micron-sized powders is due to the $\alpha_{Al\rightarrow Al(OH)3}$(t) formation during ageing. Initially, after the aluminum hydroxide formation, the reduced passivation action of this material yields Al core corruption. The latter is a self-limiting phenomenon. The $Al(OH)_3$ shell growth gradually builds-up a protective layer hindering further active metal content losses (as evidenced by the μAl mass and C_{Al} trends reported in the Figure 8 for t ≥ 168 hrs.). In particular, considering the limiting cases of bayerite (ρ = 2500 kg/m^3) and bohemite (ρ = 3080 kg/m^3), the $Al(OH)_3$ thickness over the metal core of the micron-sized particles at t = 168 hrs. can be estimated by the Eq. 2, considering the corresponding C_{Al} and the powder particle size (D_{43} and D_{32}) of the Table 3. The achieved results, show a limiting $Al(OH)_3$ shell thickness in the range 0.5 to 1.0 μm for μAl-30, and between 0.3 and 0.5 μm for μAl-7.5. It is interesting to note that in both cases, the passivation layer thickness for both the micron-sized powders exceeds the average particle size of the nAl-100 and of the nAl-40. Thus, these powders cannot be passivated during the Al→$Al(OH)_3$ conversion, and the C_{Al} is highly compromised (indeed, completely consumed).

For nano-sized aluminum powders, no significant reactivity changes are identified for the earlier phases of the ageing process (see Table 9). After 24 hours of ageing, the nAl-100 features no relevant variations of the Δm_0 and of the $T_{onset,1}$, with respect to the fresh powder. The $\alpha_{Al\rightarrow Al2O3}$(1223 K) of the powder shows a decrease from the initial value of (86.0 ± 1.1)% to (82.5 ± 1.5)% after 24 hours of ageing. This result is caused by a minor reactivity loss in both the first and the second oxidation stages of the powder. Passing to the ageing times of 27 and 72 hours, the main

phenomenon in the TG trace is the specimen mass loss (see Table 9). The achieved Δm_0 agrees with the value corresponding to $Al(OH)_3$ dehydration to Al_2O_3 [30]. As a result, during heating the scant Al core is surrounded by a relatively thick alumina layer, hindering the residual metal oxidation. A similar behavior is observed also for the nAl-40. Also in this case, from 7 hrs. of ageing on, the powder shows a mass loss as the main TG evidence, without alterations of the intense oxidation onset temperature. In this case, a minor reactivity loss in terms of $T_{onset,1+}$ characterizes the finer nAl. For nAl-40, the initial $T_{onset,1+}$ passes from (742.7 ± 1.1) K for the fresh powder, to (749.4 ± 1.2) K after 7 hrs. of ageing This is a possible (minor) effect of the increased passivation layer induced by the ageing, after $Al(OH)_3$ dehydration. The nAl-40 shows $\alpha_{Al\rightarrow Al2O3}$ reduction in both oxidation steps. For the longest ageing time considered in the study (72 hrs. for nAl-100, and 24 hrs. for nAl-40), the nearly complete metal content consumption due to ageing implies a loss of the identification of the intense oxidation onset temperature, and a lowering of the $\alpha_{Al\rightarrow Al2O3}$(1223 K) as the ageing time increases.

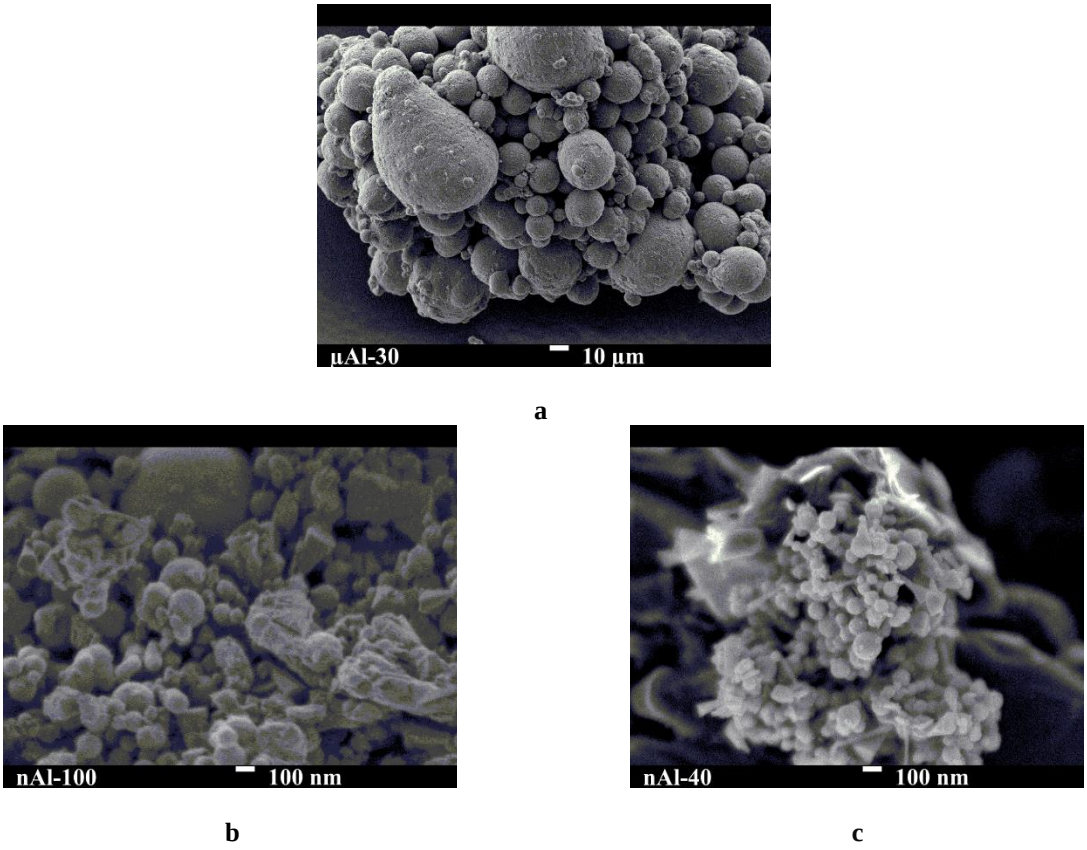

Figure 9. SEM images of H1-aged samples (a) µAl-30 (7 days), (b) nAl-100 (30 hrs.) and (c) nAl-40 (7 hrs.). Note the change in the powder appearance with respect to the SEM images of Figure 4 and Figure 5.

4. Conclusions and Future Developments

In this work, the effects of accelerated ageing on the reactivity of micron- and nano-sized powders were investigated. Two different conditions were considered, D1 (RH < 10%, 333 K) and H1 [RH = (80.2 ± 0.4)%]. In both D1 and H1, ageing was accelerated by T = 333 K. The starting characteristics of the tested powders were investigated in details, and their evolution in time was monitored during the ageing.

Powders stored in the D1 condition showed no marked changes of their characteristics over a period of 14 days (see Table 5). This was due to the low RH, granting a slow powder-environment interactions occurring (eventually) over storage times longer than the one considered in the study. The storage under humid conditions (H1), highlighted

differences between micron- and nano-sized powders. Both μAl-30 and μAl-7.5 show similar $C_{Al}(t)$ with a decrease between ageing time t = 0 and t = 168 hrs. This decrease is then followed by stable metal content and $\alpha_{Al\rightarrow Al(OH)3}(t)$, for 168 hrs. $\leq t \leq$ 336 hrs., as shown in the Figure 8. This trend is lost with the nano-sized powders, whose C_{Al} decreases monotonically reaching limiting values of nearly 2% in 72 hours (nAl-100), and 24 hours (nAl-40). The powder modifications are mainly due to the active aluminum corruption by H_2O oxidation, yielding the formation of different aluminum hydroxide polymorphs (see Table 6 and Table 7). The TG reactivity of the powders seems not significantly affected by the ageing in terms of $T_{onset,1}$, when an intense oxidation can be recognized. On the other hand, the $\alpha_{Al\rightarrow Al2O3}$ shows a monotonic decrease for increasing ageing time. This behavior is due to the $Al\rightarrow Al(OH)_3$ conversion during ageing. The reduced reactivity of aged powders is due to the corruption of the pristine Al_2O_3 passivation layer in the humid environment. When the amorphous oxide passivation layer is compromised, a sequence of events is started. First, diffusion of oxidizing species toward the core of the particles consumes active metal. Second, $Al(OH)_3$ is formed upon metal reaction with water vapor. When tested at low heating rates, the hydroxide turns to Al_2O_3 [30]. The so formed alumina layer features a relatively high thickness, hindering oxidizing species diffusion toward the residual metal core. Finally, it can be noted that during the storage in the humid environment, a limiting $Al(OH)_3$ thickness in the range 0.3 to 1 μm is reached. Nano-sized aluminum mean particle size is typically finer than this limiting size. Thus, the $Al(OH)_3$ cannot passivate the surface of nAl powders, thus explaining the complete consumption of their metal content during storage in a humid environment.

Future developments of this work will focus on a deeper investigation of the thermal behavior of the aluminum powders for points of incipient change of the disperse system characteristics, and on an evaluation of the effects of higher heating rates on the thermal behavior of the aged materials.

Acknowledgement

This work is partially financed by the GRAIL (Green Advanced High Energy Propellants for Launchers) H2020 program (EU grant agreement no. 638719).

Authors thank Dr. Gianluigi Marra (ENI, Centro Ricerche per le Energie Rinnovabili e l'Ambiente, Novara, Italy) for XRD, SEM and TEM data and helpful discussions.

References

[1] A.V. Grosse, J.B. Conway, Combustion of metals in oxygen, Ind. Eng. Chem. 50 (1958) 663–672. doi:10.1021/ie50580a040.

[2] L.T. DeLuca, L. Galfetti, F. Maggi, G. Colombo, C. Paravan, A. Reina, S. Dossi, M. Fassina, A. Sossi, Characterization and combustion of aluminum nanopowders in energetic systems, in: Met. Nanopowders Prod. Charact. Energ. Appl., 2014: pp. 301–410. doi:10.1002/9783527680696.ch12.

[3] C. Paravan, F. Maggi, S. Dossi, G. Marra, G. Colombo, L. Galfetti, Pre-burning characterization of nanosized aluminum in condensed energetic systems, in: Energ. Nanomater. Synth. Charact. Appl., 2016: pp. 341–368. doi:10.1016/B978-0-12-802710-3.00013-1.

[4] E.W. Price, Combustion of metallized propellants, in: K.K. Kuo, M. Summerfield (Eds.), Fundam. Solid Propellant Combust., AIAA Progress in Aeronautics and Astronautics, Vol. 90, 1984: pp. 479–513. doi: 10.2514/5.9781600865671.0515.0598.

[5] G.A. Risha, B.J. Evans, E. Boyer, K.K. Kuo, Metals, energetic additives, and special binders used in solid fuels for hybrid rockets, in: Fundam. Hybrid Rocket Combust. Propuls., 2007: pp. 413–457. doi:10.2514/4.866876.

[6] A. Sossi, E. Duranti, M. Manzoni, C. Paravan, L.T. Deluca, A.B. Vorozhtsov, M.I. Lerner, N.G. Rodkevich, A.A. Gromov, N. Savin, Combustion of HTPB-based solid fuels loaded with coated nanoaluminum, Combust. Sci. Technol. 185 (2013) 17–36. doi:10.1080/00102202.2012.707261.

[7] M.A. Trunov, M. Schoenitz, E.L. Dreizin, Ignition of aluminum powders under different experimental conditions, Propellants, Explos. Pyrotech. 30 (2005) 36–43. doi:10.1002/prep.200400083.

[8] A.P. Ilyin, A.A. Gromov, V. An, F. Faubert, C. De Izarra, A. Espagnacq, L. Brunet, Characterization of aluminum powders I. Parameters of reactivity of aluminum powders, Propellants, Explos. Pyrotech. 27 (2002) 361–364. doi:10.1002/prep.200290006.

[9] A.A. Gromov, A.P. Ilyin, U. Förter-Barth, U. Teipel, Characterization of aluminum powders: II. Aluminum nanopowders passivated by non-inert coatings, Propellants, Explos. Pyrotech. 31 (2006) 401–409. doi:10.1002/prep.200600055.

[10] A. Sossi, E. Duranti, C. Paravan, L.T. DeLuca, A.B. Vorozhtsov, A.A. Gromov, Y.I. Pautova, M.I. Lerner, N.G. Rodkevich, Non-isothermal oxidation of aluminum nanopowder coated by hydrocarbons and

fluorohydrocarbons, Appl. Surf. Sci. 271 (2013) 337–343. doi:10.1016/j.apsusc.2013.01.197.
[11] B.J. McBride, S. Gordon, Computer program for calculation of complex chemical equilibrium compositions and applications, NASA Ref. Publ. 1311. (1994) 184. doi:NASA RP-1311.
[12] N. Kubota, Propellants and Explosives: Thermochemical Aspects of Combustion, 3rd ed., Wiley-VCH, Weinheim, Germany, 2015. doi:10.1002/9783527693481.
[13] A.M. Karabeyoglu, B.J. Evans, Effect of "O/F Shift" on combustion efficiency, AIAA Paper No. 2014-3851 (2014). doi:10.2514/6.2014-3851.
[14] L.T. DeLuca, L. Galfetti, G. Colombo, F. Maggi, A. Bandera, V.A. Babuk, V.P. Sinditskii, Microstructure effects in aluminized solid rocket propellants, J. Propuls. Power. 26 (2010) 724–732. doi:10.2514/1.45262.
[15] V.A. Babuk, V.A. Vassiliev, V. V Sviridov, Formation of condensed combustion products at the burning surface of solid rocket propellant, in: AIAA, 2000: pp. 749–776. doi:10.2514/5.9781600866562.0749.0776.
[16] C. Paravan, Ballistics of Innovative Solid Fuel Formulations for Hybrid Rocket Engines, PhD Dissertation, Politecnico di Milano (2012).
[17] L.T. DeLuca, L. Galfetti, F. Severini, L. Meda, G. Marra, A.B. Vorozhtsov, V.S. Sedoi, V.A. Babuk, Burning of nano-aluminized composite rocket propellants, Combust. Explos. Shock Waves. 41 (2005) 680–692. doi:10.1007/s10573-005-0080-5.
[18] E.M. Popenko, A.P. Ilyin, A.M. Gromov, S.K. Kondratyuk, V.A. Surgin, A.A. Gromov, Combustion of mixtures of industrial aluminum powders with superfine powders of aluminum and aluminum oxide in air, Combust. Explos. Shock Waves. 38 (2002) 157–162. doi:10.1023/A:1014994630495.
[19] M. Cliff, F. Tepper, V. Lisetsky, Ageing characteristics of Alex® nanosize aluminium, AIAA Paper No. 2001-3287 (2001). doi:10.2514/6.2001-3287.
[20] Y. Li, W. Song, C. Xie, D. Zeng, A. Wang, M. Hu, Influence of humidity on the thermal behavior of aluminum nanopowders, Mater. Chem. Phys. 97 (2006) 127–131. doi:10.1016/j.matchemphys.2005.07.064.
[21] O.B. Nazarenko, Y.A. Amelkovich, A.I. Sechin, Characterization of aluminum nanopowders after long-term storage, Appl. Surf. Sci. 321 (2014) 475–480. doi:10.1016/j.apsusc.2014.10.034.
[22] S. Pisharath, F. Zhang, H.G. Ang, Influence of passivation on ageing of nano-aluminum: Heat flux calorimetry and microstructural studies, Thermochim. Acta. 635 (2016) 59–69. doi:10.1016/j.tca.2016.04.022.
[23] Q.S.M. Kwok, R.C. Fouchard, A. Turcotte, P.D. Lightfoot, R. Bowes, D.E.G. Jones, Characterization of aluminum nanopowder compositions, Propellants, Explos. Pyrotech. 27 (2002) 229-240. doi:10.1002/1521-4087(200209)27:4<229::AID-PREP229>3.0.CO;2-B.
[24] D.E.G. Jones, R. Turcotte, R.C. Fouchard, Q.S.M. Kwok, A.M. Turcotte, Z. Abdel-Qader, Hazard characterization of aluminum nanopowder compositions, Propellants, Explos. Pyrotech. 28 (2003) 120–131. doi:10.1002/prep.200390018.
[25] Y.S. Kwon, A.A. Gromov, J.I. Strokova, Passivation of the surface of aluminum nanopowders by protective coatings of the different chemical origin, Appl. Surf. Sci. 253 (2007) 5558–5564. doi:10.1016/j.apsusc.2006.12.124.
[26] S. Cerri, M. A. Bohn, K. Menke, L. Galfetti, Ageing behaviour of HTPB based rocket propellant formulations, Cent. Eur. J. Energ. Mater. 6 (2009) 149–165. doi:10.1002/prep.201200186.
[27] Y.F. Ivanov, M.N. Osmonoliev, V.S. Sedoi, V.A. Arkhipov, S.S. Bondarchuk, A.B. Vorozhtsov, A.G. Korotkikh, V.T. Kuznetsov, Productions of ultra-fine powders and their use in high energetic compositions, Propellants, Explos. Pyrotech. 28 (2003) 319–333. doi:10.1002/prep.200300019.
[28] S. Brunauer, P.H. Emmett, E. Teller, Adsorption of gases in multimolecular layers, J. Am. Chem. Soc. 60 (1938) 309–319. doi: 10.1021/ja01269a023.
[29] L.P.H. Jeurgens, W.G. Sloof, F.D. Tichelaar, E.J. Mittemeijer, Growth kinetics and mechanisms of aluminum-oxide films formed by thermal oxidation of aluminum, J. Appl. Phys. 92 (2002) 1649–1656. doi:10.1063/1.1491591.
[30] T. Sato, Thermal decomposition of aluminum hydroxides, J. Therm. Anal. 32 (1987) 61–70. doi:10.1007/BF01914548.